ADVANCED FUNCTIONAL MATERIALS
www.afm-journal.de

Full Depth-of-Discharge Cycling in Zn||MnO_2 Batteries Enabled by Alkaline Salt-Concentrated Hydrogel Electrolyte

Mingqian Li, Simon Danitz, John Holoubek, Guorui Cai, Jordan Shawn Lee, Haozhe Zhang, Wenqing Lu, Junlin Wu, Xueying Quinn, Jon Truskier, Sasha Gorer, Ying Shirley Meng, and Zheng Chen**

Alkaline Zn||MnO_2 batteries hold great potential for grid energy storage due to their material abundance, low cost, and high safety. However, their large-scale application is limited to primary cells because of poor cycle stability, which is caused by hydrogen evolution on Zn anode and irreversible phase transitions of MnO_2 cathode. Herein, it develops alkaline salt-concentrated hydrogel electrolytes that combine the benefits of both high-concentration and hydrogel electrolytes. These electrolytes with high ionic conductivity of 370 mS cm^{-1} selectively block Zn^{2+} crossover, prevent MnO_2 phase transitions, and mitigate parasitic reactions by tightly binding and confining salt-coordinated water within the hydrogel matrix. Consequently, Zn||MnO_2 cells with high mass loading of 82 mg cm^{-2} exhibit minimal capacity loss after 1200 cycles. Additionally, reversible 100% depth-of-discharge cycling is demonstrated, leading to a fivefold increase in cell energy density. This work provides a cost-effective and highly rechargeable solution for large-scale grid energy storage.

1. Introduction

The widespread adoption of clean and renewable energy demands affordable, long-lasting, and safe grid energy storage solutions. Traditional pumped hydro storage is hindered by geographical and land-use constraints, making it inadequate for supporting rapid grid energy storage expansion.[1] While portable lithium-ion batteries (LIBs) offer high energy density, they are expensive and pose inherent safety risks, making them unsuitable for large-scale grid energy storage.[2–6] To address this gap, extensive research has focused on aqueous Zn||MnO_2 batteries, due to their high theoretical capacity, material abundance, and excellent safety properties.[7–10] However, their lifespan is curtailed by issues such as parasitic hydrogen evolution reaction (HER), Zn^{2+} crossover, and irreversible phase transitions in the MnO_2 cathode.

The alkaline battery market is a significant and steadily growing part of the global battery industry, projected to reach USD 13.70–14.43 billion by 2032–2033 (CAGR 5.03–5.84%) due to rising demand for consumer electronics, emergency backup solutions, and advancements in recyclable battery technologies.[11] Alkaline Zn||MnO_2 primary batteries, a key component of this market, have long been a reliable power source for electronic devices due to their impressive shelf life, coupled with high power density and relatively broad potential window.[12,13] This performance is attributed to favorable kinetics and reduced HER activity compared to those in natural to mildly acidic systems.[14–16] However, the limited cycle life hinders their effective application as secondary (rechargeable) batteries. The degradation mechanism in alkaline systems remains a topic of debate. Typically, the electrodes prefer to undergo conversion reactions in strongly basic conditions, where Zn is converted to ZnO while MnO_2 is converted to MnOOH or $Mn(OH)_2$ during discharge, and reversed during charge.[17] Although the 1-electron reaction (Equation 1) of MnO_2 with a shallow depth-of-discharge (DoD) can enhance cycle stability, it significantly reduces the specific capacity and energy density.[18] While capacity utilization can be increased by further reducing the MnO_2 cathode (Equation 2), it renders Zn^{2+} crossover in highly alkaline electrolytes, triggering irreversible phase transitions. Zincate formed during discharge

M. Li, J. Holoubek, G. Cai, J. S. Lee, W. Lu, J. Wu, X. Quinn, Z. Chen
Aiiso Yufeng Li Family Department of Nano and Chemical Engineering
University of California San Diego
9500 Gilman Drive, La Jolla, CA 92093, USA
E-mail: caiguorui@ustc.edu.cn; zhc199@ucsd.edu

S. Danitz, J. Wu, Z. Chen
Program of Materials Science and Engineering
University of California San Diego
9500 Gilman Drive, La Jolla, CA 92093, USA

G. Cai
Hefei National Research Center for Physical Sciences at the Microscale
University of Science and Technology of China
Hefei, Anhui 230026, China

H. Zhang, Y. S. Meng
Pritzker School of Molecular Engineering
University of Chicago
Chicago, IL 60637, USA

J. Truskier, S. Gorer
Zelos Energy
1933 Davis, Suite 297, San Leandro, CA 94577, USA

Z. Chen
Sustainable Power & Energy Center (SPEC)
University of California San Diego
9500 Gilman Drive, La Jolla, California 92093, USA

The ORCID identification number(s) for the author(s) of this article can be found under https://doi.org/10.1002/adfm.202508361

DOI: 10.1002/adfm.202508361

can migrate to the cathode. It reacts with Mn^{3+} intermediates to form insulating and irreversible compounds such as Mn_3O_4 and $ZnMn_2O_4$.[19,20] These compounds decrease in electronic conductivity by several orders of magnitude and disrupt the MnO_2 structure, resulting in severe capacity loss.[21] In addition, the dissolution of zinc, coupled with hydrogen generation, is thermodynamically favorable in a strongly alkaline environment. This parasitic HER depletes zinc and water, builds internal gas pressure, and causes capacity decay, raising safety concerns and diminishing the viability of alkaline Zn||MnO_2 cells.

1-electron reaction:

$$MnO_2 + H_2O + e^- \rightarrow MnOOH + OH^- \quad (1)$$

2-electron reaction:

$$MnOOH + H_2O + e^- \rightarrow Mn(OH)_2 + OH^- \quad (2)$$

To address the aforementioned issues, various strategies such as solvation structure regulation, interface engineering and failure mechanism were extensively investigated.[22–24] Gel-polymer electrolytes (GPEs) have gained recent attention due to their high flexibility, stability, and safety. For instance, Leng et al. developed a polyzwitterionic hydrogel electrolyte design to regulate water activity and ensure uniform ion distribution.[25] Similarly, Chen et al. employed a cellulose-based hydrogel to mitigate Zn dendrite formation and enable a wide operational temperature range from −40 to 60 °C.[26] In addition, polyacrylic acid (PAA)-based hydrogels have shown promise for extending cycle life and increasing operating voltage, although most of the studies focus on neutral electrolyte systems.[27,28] Given the limited research on alkaline environments,[29] systematic investigations into the degradation mechanisms of Zn||MnO_2 batteries with GPEs in strong alkaline environments are essential for enhancing their performances.

Here, we selected PAA as the polymer model for the investigation of alkaline GPEs, which is a widely utilized and scalable gel polymer electrolyte in zinc-air and neutral zinc-ion batteries.[30–32] The PAA-based GPEs were coupled with a commercial MnO_2-Bi_2O_3-Cu cathode featuring a high mass loading of up to 82 mg cm^{-2} to systematically investigate its effect on HER suppression, cathode degradation, Zn^{2+} crossover, and cycling behavior in strongly alkaline environments. Cu and Bi_2O_3 additives critically enhance the kinetics and cycling stability of high-mass-loading MnO_2 cathodes in alkaline MnO_2-Zn batteries by forming reversible Bi-Mn and Cu-Mn complexes, which improve electronic conductivity, reduce charge-transfer resistance, and stabilize the MnO_2 structure through Bi^{3+} intercalation into the MnO_2 lattice to form birnessite, thereby suppressing irreversible Mn_3O_4 formation, preventing Mn^{3+} diffusion and disproportionation, and enabling the full two-electron redox capacity.[33,34] Our findings reveal that the alkaline salt-concentrated GPEs (ASC-GPEs) limit the number and availability of water molecules by creating hydrogen bonding between salt coordinated water and the polymer skeleton. This not only suppresses HER activity by reducing available water but also hinders the formation of irreversible phases due to Zn^{2+} crossover. Consequently, the cycling performance of Zn||MnO_2 pouch cells experiences a significant improvement, especially under shallow DoD (20%), with this enhancement maintained over 1200 cycles. The evolution of phase compositions, electrode morphology, and element distribution over cycling was systematically characterized to identify the capacity degradation mechanism in both conventional aqueous solution and ASC-GPE systems. The ASC-GPE with 9 M KOH demonstrated improved long-term cycling performance even at 100% DoD, advancing the potential of alkaline Zn||MnO_2 batteries for grid energy storage.

2. Results and Discussion

Figure 1a highlights the advantages of ASC-GPEs compared to traditional high-concentration electrolytes (HCEs) and GPEs. While increasing KOH salt concentrations to form HCEs enhances ionic conductivity, improves kinetics, and reduces the mobility and quantity of free water to some extent, it has limited impact on suppressing the accessibility and mobility of free water molecules formed during the de-solvation process on the Zn surface. Conversely, although GPEs restrict the mobility of free water molecules on the surface of Zn, it suffers from poor conductivity performance. The introduction of ASC-GPEs addresses both issues by reducing the availability and activity of water molecules. Consequently, this approach can help in limiting the thermodynamically favorable HER process, as shown in Figure 1b. To prove the concept, a typical ASC-GPEs was prepared and the schematic in Figure S1 (Supporting Information) shows the synthesis process of the alkaline PAA-based GPEs. Acrylic acid is polymerized by using potassium persulfate (KPS) and N,N′-methylenebisacrylamide (MBAA) as the initiator and crosslinker, respectively.[30] With a simple polymerization-soaking process, PAA-based GPEs with different concentrations of KOH can be prepared in large quantities (i.e., ≈10 g, inset in **Figure 2a**). The ionic conductivities of GPEs soaked in different KOH concentrations are measured based on the method in the experimental section and presented in Figure 2a. The ionic conductivity increases from 151 to 370 mS cm^{-1} at room temperature as the concentrations of KOH increase from 3 to 9 M (simplified as PAA-9 M KOH gel). A maximum conductivity of ≈500 mS cm^{-1} is reached at 50 °C by the PAA-9 M KOH gel. The steady increase in ionic conductivity with higher concentration and temperature suggests that, unlike regular alkaline solutions, ion movement in PAA-based gel electrolytes likely occurs through ion hopping or segmental motion along the gel structure.[35]

Fourier-transform infrared (FT-IR) spectroscopies of PAA-based GPEs were collected (Figure 2b) to examine the O—H bonding conditions. The O—H stretch band (2600–3800 cm^{-1}) was deconvoluted into five sub-bands, representing hydrogen-bonded and non-hydrogen-bonded water molecules.[36] As KOH concentration increases from 3 to 9 M in the PAA-based GPEs, the ratio of free O—H vibrations decreases from 10.05% to 7.48%, indicating fewer free water molecules are available for potential hydrogen evolution. This was also confirmed by Raman spectra. Figure S2 (Supporting Information) shows that both 9 M KOH and PAA-9 M KOH have strong K^+–OH^- interactions. In the PAA gel, the increased signal from weakly bonded water suggests that water interacts with the PAA structure. Furthermore, a corrosion potential from −0.0159 V Zn/Zn^{2+} to −0.0285 V Zn/Zn^{2+} was observed (Figure 2d) when replacing 9 M KOH solution with the PAA-9 M KOH gel, suggesting that zinc corrosion is also suppressed by inhibiting the HER. Both FT-IR and corrosion test results are

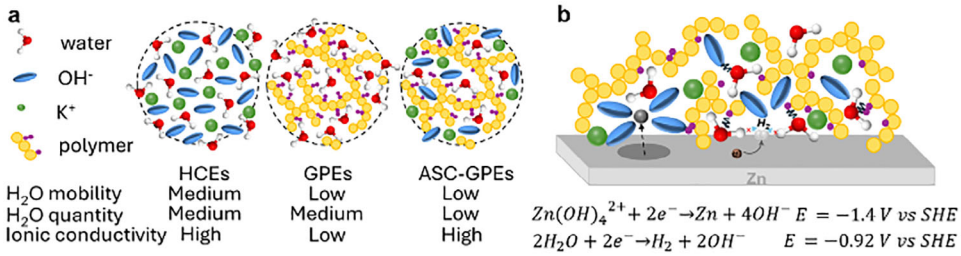

Figure 1. a) Schematic showing the comparisons between traditional HCEs, GPEs and ASC-GPEs in terms of H_2O mobility, free H_2O quantity and ionic conductivity. b) Mechanism of ASC-GPEs to suppress the HER activity.

confirmed further by the density functional theory (DFT) calculation results in Figure 2c. The interaction energy (E_{int}) between two water molecules (W-W) is −0.363 eV, while it is −0.735 eV between water and the terminal hydroxy group of PAA (W-PAA). These robust W-PAA interactions effectively constrain water molecules, playing a key role in suppressing HERs.

Gas chromatography (GC) measurements were conducted to identify the gas generation during cycling of the alkaline Zn||MnO_2 batteries (Figure S3, Supporting Information). The lowest volume of hydrogen was detected for systems equipped with PAA-9 M KOH gel. The gas volume was recorded at different cycling points for both 9 M KOH solution and PAA-9 M KOH gel to monitor hydrogen evolution (Figure 2e). Cells with ASC-GPEs generated less hydrogen at a slower rate than those with HCEs.

Figure 3a illustrates the long-term cycling stability of alkaline Zn||MnO_2 batteries with different electrolyte systems. Cells with the PAA-6 M KOH gel exhibited nearly double the cycle life (≈400 cycles at 20% DoD) compared to those with the 9 M KOH solution. Furthermore, cells with ASC-GPEs (PAA-9 M KOH gel)

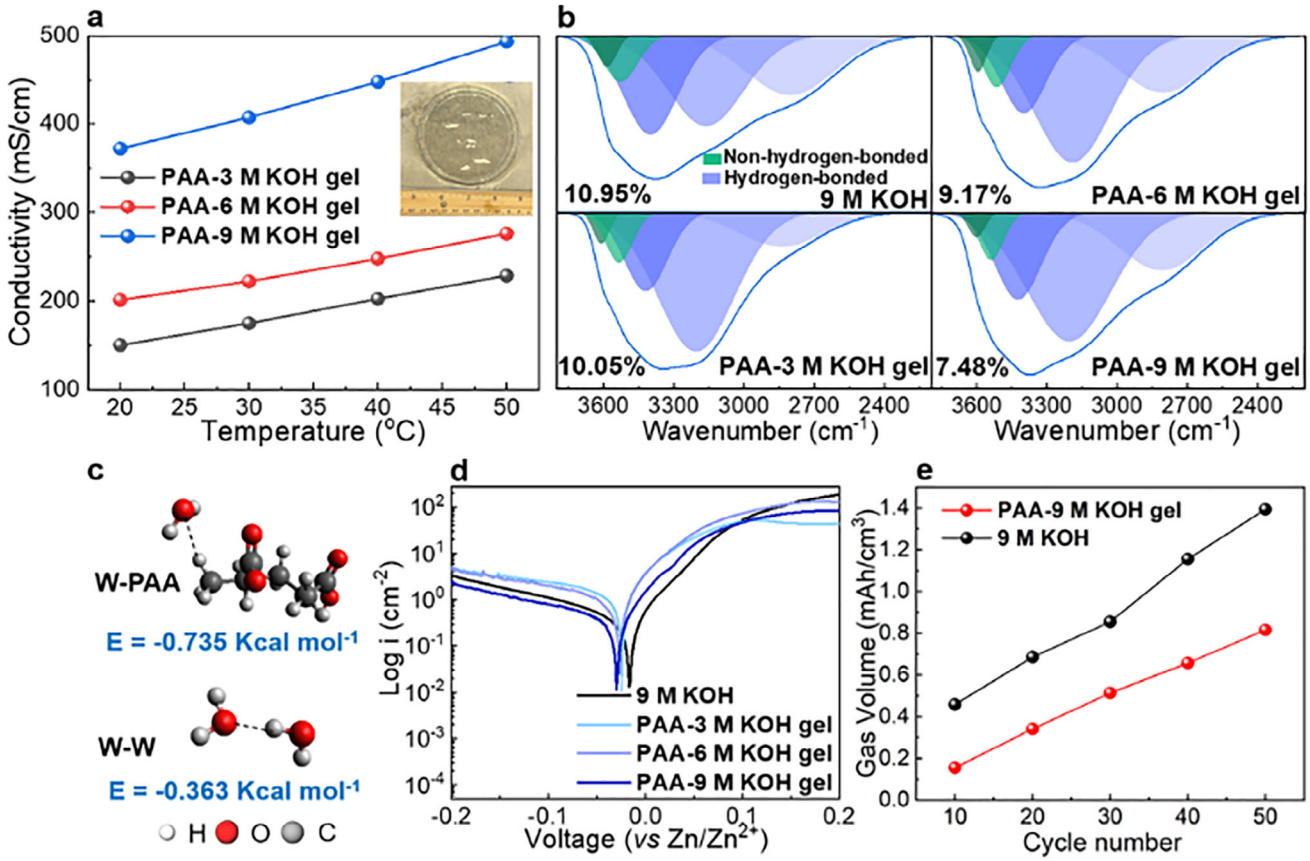

Figure 2. a) Ionic conductivities of the PAA-based GPEs with a concentration of 3, 6, and 9 M KOH, respectively, at different temperatures. The inset figure shows the as-prepared PAA-9 M KOH gel. b) FT-IR spectra observed in the range of 2300–3800 cm^{-1} corresponding to the O—H stretching modes of water for different electrolyte systems. c) Molecular models used to simulate interactions between water molecules and surrounding water and terminal groups from PAA. d) Tafel plots obtained for the 9 M KOH solution and PAA-based GPEs with different KOH concentrations at a scan rate of 2 mV s^{-1}. e) The gas volume per mAh per cm^3 on cycling for both the 9 M KOH solution and PAA-9 M KOH gel.

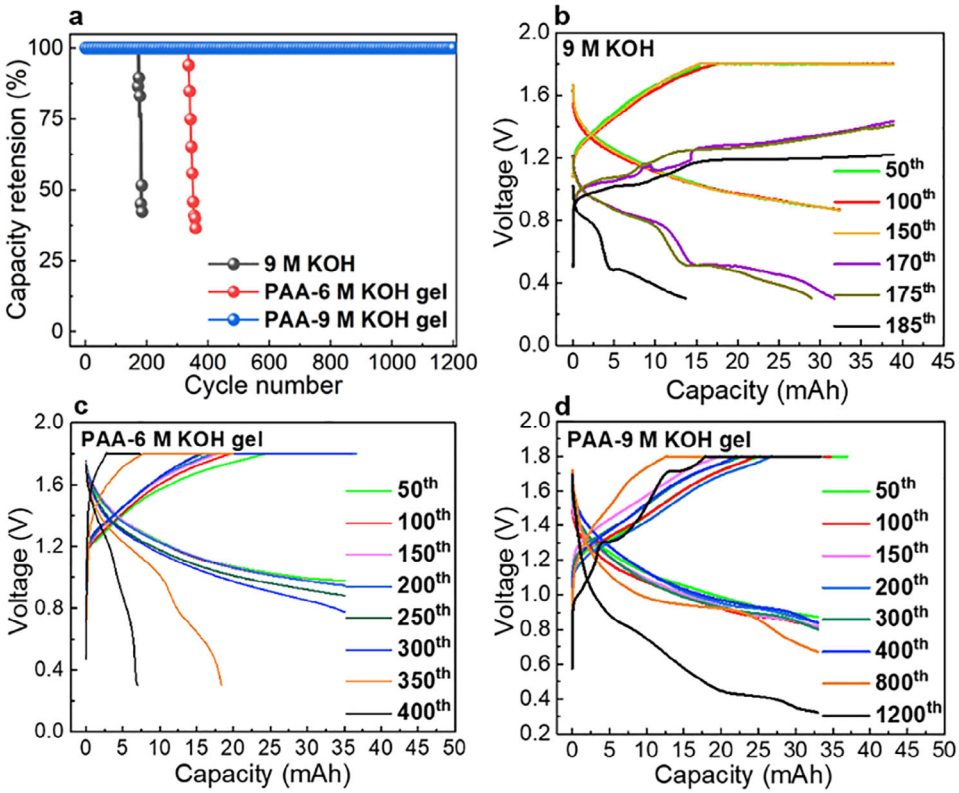

Figure 3. Long-term cycling performance comparison a) and charge/discharge curves b-d) of Zn||MnO_2 cells with different electrolyte systems with 9 M KOH solution, PAA-6 M KOH gel, and PAA-9 M KOH gel.

showed no noticeable capacity degradation after 1200 cycles, highlighting the benefits of integrating both HCEs and GPEs. Charging-discharging behaviors for different electrolyte systems are detailed in Figure 3b–d. Initially, negligible differences appeared between the HCEs and GPEs systems in the cycling window of 0.3 to 1.8 V. When cells were cycled in the HCEs system, their discharge curves continued to descend with the increase of an extra plateau, eventually hitting the cut-off voltage at 0.3 V. On the contrary, no noticeable changes were observed in the discharge curve for those with our ASC-GPEs systems, which presented two reversible discharge plateaus akin to those for H^+ and Zn^{2+} co-insertion/extraction. Initially, proton intercalation dominated with good reversibility during the first few hundred cycles as only 10% DoD was utilized, resulting in a characteristic slope region (above 1 V vs Zn/Zn^{2+}). The appearance of the inflection point ≈0.9 V at prolonged cycling (≈400 cycles) indicated further conversion of MnOOH into Mn_3O_4 or $Mn(OH)_2$, which was followed by an acceleration of a larger overpotential with a lower and shorter plateau succeeded by a Zn^{2+} insertion region (1200 cycle, 0.4 to 0.8 V).[34,37] An extra plateau at ≈0.4 V was detected, which might be attributed to redox capacity from Bi_2O_3 and Cu additives.[19] Although the facile H^+ insertion with faster kinetics due to its smaller ion radius is always preferred, the Zn^{2+} insertion is inevitable due to the presence of Zn^{2+} and will ultimately lead to the generation of electrical insulated phase.

To illustrate the decay mechanism of alkaline Zn||MnO_2 batteries within different electrolyte systems, the cycled cathodes were characterized by X-ray diffraction (XRD) (**Figure** 4a,b). After 50 cycles, MnOOH was detected as an intermediate in the HCEs, which confirms the "1-electron reaction mechanism" of MnO_2.[38] For the shallow DoD cycling process, new phases such as ZnO and $ZnMn_2O_4$ appeared after 180 cycles on the cathode with characteristic peaks of ZnO (34.3°, 36.2°) and $ZnMn_2O_4$ (29.3° and 33.0°).[39,40] This indicates Zn^{2+} ion crossover after 1200 cycles, which could be the primary cause of capacity degradation. The XRD profile of the gel system supports this hypothesis (Figure 4b). After 250 cycles, no ZnO and $ZnMn_2O_4$ signals were observed. Instead, Mn compounds with intermediate valences, such as Mn_2O_3 and Mn_3O_4, were detected, indicating a reduction in the average Mn valence.[41,42] After a long-term cycle (1200 cycles), a bismuth-manganese oxide phase (ICDD-00-043-0185) and $ZnMn_2O_4$ were detected. The formation of the bismuth-manganese oxide can compete with the formation of $ZnMn_2O_4$ to slow down the loss of capacity due to irreversible phase conversion of later. To further confirm these observations, scanning electron microscopy (SEM) and energy dispersive X-ray spectroscopy (EDS) were performed. Although there were no significant morphology variations observed in cathodes cycled under different conditions (Figures S4 and S5, Supporting Information), the cross-section EDS results clearly show that zinc ions were present in the cathodes even after only 50 cycles in HCEs (Figures S6 and S7, Supporting Information).

The X-ray photoelectron spectroscopy (XPS) results further solidify the differences in Mn phases. The Mn *2p* and Zn *2p* XPS spectra are shown in Figure 4c,d for both electrolyte systems. The Mn *2p* peak at 642 eV was deconvoluted based on the

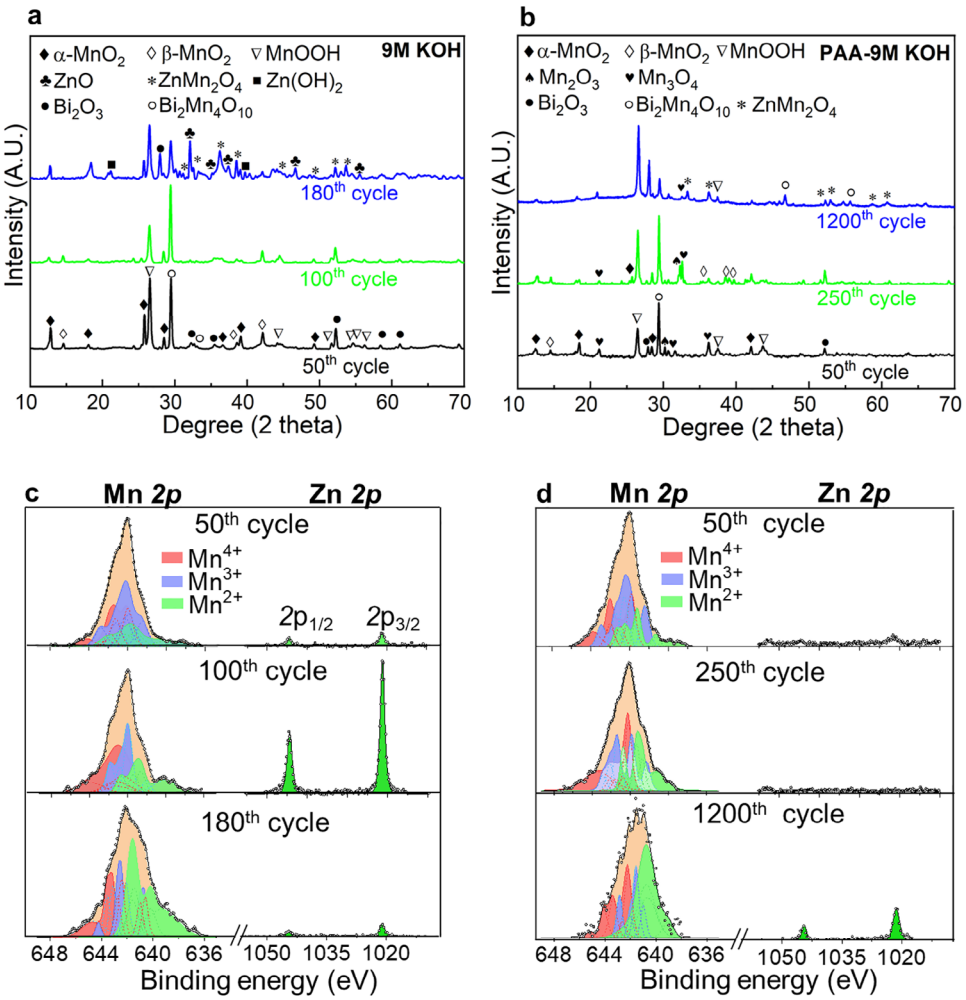

Figure 4. a,b) XRD and c,d) XPS profiles of MnO_2 cathodes with (a, c) alkaline aqueous and (b, d) ASC-GPE systems after different cycles.

characteristic peaks for different valences.[43] As cycling progressed, the proportion of Mn^{2+} increased, reaching ≈50% in the degraded cathode of aqueous solution systems after 180 cycles. In contrast, the Mn^{2+} ratio rose modestly from 21.6% to 30.5% even at 250 cycles, indicating reduced phase degradation for those of ASC-GPEs. The specific ratios of Mn valences at different cycling stages are summarized in **Table 1**. A more distinct comparison is observed in the Zn *2p* spectra.[44] No signal was detected on cathodes cycled with ASC-GPEs, while a signal was clearly present in those with HCEs after 50 cycles.

The appearance of impurities such as zinc and low-valence manganese phases on cathodes serves as a signal of capacity degradation. To correlate the characterizations with electrochemical behaviors, 3-electrode pouch cells were fabricated to monitor the potential variations during cycles by using a Ni foil as the reference electrode. **Figure** 5a,b shows the potential shift of cathodes in the HCEs and ASC-GPEs systems, respectively. The discharge curve gradually shifted downward over cycles. For the cell using PAA-9 M KOH gel, a minimal drop of 9.5 mV was observed after 50 cycles(inset in Figure 5b), significantly lower than the drop of

Table 1. Ratios of Mn valence after different cycle conditions.

Cathode materials	Mn^{2+}	Mn^{3+}	Mn^{4+}
9 M KOH at 50th cycle	23.43%	44.72%	31.85%
9 M KOH at 100th cycle	26.69%	30.84%	42.72%
9 M KOH at 180th cycle	48.97%	23.39%	27.63%
PAA-9 M KOH gel 50th cycle	21.62%	42.78%	35.62%
PAA-9 M KOH gel at 250th cycle	30.46%	34.07%	35.47%
PAA-9 M KOH gel at 1200th cycle	47.25%	22.78%	29.77%

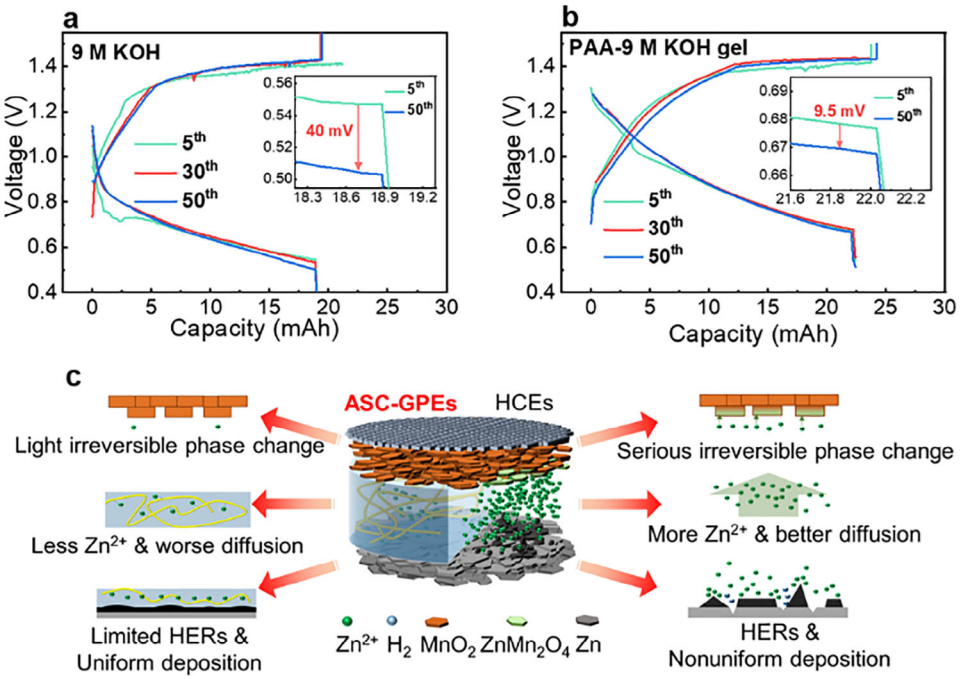

Figure 5. Charge-discharge curves of 3-electrode pouch cells with a) HCEs and b) ASC-GPEs systems. c) Schematic showing the battery degradation mechanisms with HCEs and ASC-GPEs systems.

40 mV seen with 9 M KOH solution (inset in Figure 5a) at the lower cut-off voltage. The reduced cut-off voltage (vs reference electrodes) indicates a deeper DoD necessary to obtain the same discharge capacity. This may be caused by the loss of active materials as well as the formation of irreversible phases in the alkaline electrolyte system. Such results agree with the aforementioned XRD and XPS results.

Electrochemical impedance spectroscopy (EIS) was conducted in Figure S8a,b (Supporting Information). The acquired full-cell impedance spectra can be distinguished by the bulk electrolyte resistance (R_s), anode resistance (R_{ano}), active material resistance (R_{cat}), and irreversible phase resistance (R_{irr}) (Figure S9a, Supporting Information). The R_{ano} of the cell with 9 M KOH solution continued to increase throughout cycling, which can be attributed to the non-uniform deposition of Zn/ZnO. The R_{irr} of the cell with 9 M KOH solution rose dramatically, which indicates accumulation of insulating irreversible phases (i.e., $ZnMn_2O_4$, Mn_3O_4) (Figure S9b, Supporting Information). On the other hand, the presence of ASC-GPEs inhibited the mobility of Zn^{2+} ions. The restricted mobility of Zn^{2+} in the PAA-based gel electrolyte is mainly due to its coordination with the hydroxyl-rich groups (—COO^-) in PAA, which limits ion movement. Additionally, in the concentrated KOH solution, Zn^{2+} forms complex ions like $Zn(OH)_4^{2-}$ that are larger and more negatively charged than free Zn^{2+}, further reducing their mobility in the electrolyte.

The transference number of Zn^{2+} ions decreased from t_{Zn}^{2+} = 0.312 in 9 M KOH solution to t_{Zn}^{2+} = 0.113 in PAA-9 M KOH gel, which is consistent with the result from the interaction energy calculation (Figure 2c). As a result, the R_{irr} of PAA-9 M KOH gel showed negligible variations, and no noticeable irreversible phases were found (Figure S9c, Supporting Information). The surface morphologies of cycled anodes in 9 M KOH solution after 180 cycles and PAA-9 M KOH gel after 250 cycles were constructed by Filmetrics Profilm3D (Figure S10a, Supporting Information). Compared with the anode with HCEs, zinc redeposition was more uniform with ASC-GPEs, and the height variation was reduced from 22.5 to 6 µm (Figure S10b, Supporting Information). An illustration of the influence of ASC-GPEs on the battery degradation mechanism contrasted with the HCEs is in Figure 5c. The ASC-GPEs benefit uniform Zn plating to alleviate re-distribution and/or dendrite formation and reduce the mobility of Zn^{2+} ions in the electrolyte. Therefore, the formation of the irreversible $ZnMn_2O_4$ phase is minimized. On the contrary, severe dendrite formation along with Zn^{2+} ion loss occurs in the conventional HCEs system, which triggers the irreversible phase conversion and increased discharging voltage drop.

Cells with HCEs and ASC-GPEs were cycled with 100% DoD to further evaluate their degradation mechanism. The alkaline Zn||MnO_2 battery with traditional electrolyte systems decayed dramatically and failed to survive under deep DoD, due to severe Zn^{2+} ion crossover and irreversible phase transition.[45] As shown in **Figure 6a**, although the capacity of cells with 9 M KOH solution dropped to 45.3% after 50 cycles, 85% of their initial capacity was sustained for those with ASC-GPEs. Different charging and discharging voltage profiles were also observed in both systems (Figure 6b,c). The overpotential dropped gradually and became stable after ≈30 cycles with the PAA-9 M KOH gel, while it accumulated over cycles in the 9 M KOH solution. This may result from the generation of electronically insulating $ZnMn_2O_4$ phases in the latter. Cells with a high mass loading of MnO_2 (82 mg cm^{-2}) were fabricated to further highlight the advantages of the ASC-GPEs (Figure S11, Supporting Information). The PAA-9 M KOH gel improved the cycle performance over the 9 M KOH solution by improving 30.9% capacity retention after

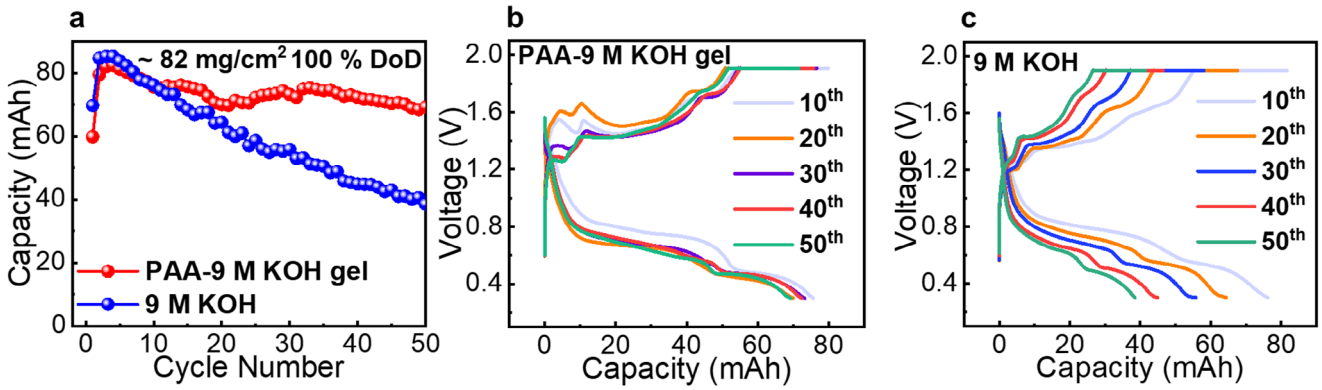

Figure 6. a) Cycling performances and b,c) charge/discharge curves of Zn||MnO_2 cells with HCEs and ASC-GPEs at 100% DoD.

50 cycles, which stands out from most of the state-of-the-art alkaline Zn||MnO_2 batteries (Table S1, Supporting Information), especially when considering full-cell-level energy and power density alongside practical factors such as cathode mass loading and specific capacity.

3. Conclusion

In conclusion, an alkaline PAA-based hydrogel electrolyte has been selected as a representative GPE to investigate the gel structure and alkaline condition effects on cycle performance and HER activity in rechargeable Zn||MnO_2 batteries. The HERs were alleviated by restricting the amount and mobility of water molecules through the integration of the advantages of HCEs and GPEs as well as the strong interactions between salt-coordinated water and the gel polymer skeleton. The capacity retention increased significantly to 1200 cycles (six times the conventional cyclability) under conventional shallow DoD (≈20%). Systematic experimental and calculation results indicate that the rapid capacity decay stems from the increased voltage hysteresis, due to Zn^{2+} crossover and irreversible phase formation at the cathode. Our salt-concentrated GPEs can successfully address these issues even under a full DoD cycling and high-mass loading operation condition.

Supporting Information

Supporting Information is available from the Wiley Online Library or from the author.

Acknowledgements

This study was partially supported by the Zelos Energy. The authors acknowledge the UCSD Crystallography Facility. A portion of the work used the UCSD-MTI Battery Fabrication Facility and the UCSD-Arbin Battery Testing Facility. The authors also acknowledge the start-up fund support from the Jacob School of Engineering at UC San Diego.

Conflict of Interest

The authors declare the following competing financial interest: A patent application titled "Deep Rechargeable Alkaline Zinc-MnO2 batteries" has been filed through the University of California San Diego Office of Innovation and Commercialization (Invention Disclosure Track: "DISC2024-01953") related to the work presented in this manuscript. Authors [Name(s)] are listed as inventors.

Data Availability Statement

The data that support the findings of this study are available from the corresponding author upon reasonable request.

Keywords

alkaline MnO_2 batteries, aqueous batteries, grid energy storage, high-concentration electrolyte, hydrogel electrolyte

Received: April 2, 2025
Revised: May 18, 2025
Published online:

[1] T. M. Gur, *Energ. Environ. Sci.* **2018**, *11*, 3055.
[2] X. Tian, Y. Yi, B. Fang, P. Yang, T. Wang, P. Liu, L. Qu, M. Li, S. Zhang, *Chem. Mater.* **2020**, *32*, 9821.
[3] P. Lyu, X. Liu, J. Qu, J. Zhao, Y. Huo, Z. Qu, Z. Rao, *Energy Storage Mater.* **2020**, *31*, 195.
[4] H. Yang, W. R. Leow, X. D. Chen, *Adv. Mater.* **2018**, *30*, 1704347.
[5] B. Liu, Y. Jia, C. Yuan, L. Wang, X. Gao, S. Yin, J. Xu, *Energy Storage Mater.* **2020**, *24*, 85.
[6] G. Cai, H. Gao, M. Li, V. Gupta, J. Holoubek, T. A. Pascal, P. Liu, Z. Chen, *Angew. Chem., Int. Ed.* **2024**, *63*, 202316786.
[7] D. Chao, C. Ye, F. Xie, W. Zhou, Q. Zhang, Q. Gu, K. Davey, L. Gu, S.-Z. Qiao, *Adv. Mater.* **2020**, *32*, 2001894.
[8] Z. Liu, L. Qin, B. Lu, X. Wu, S. Liang, J. Zhou, *ChemSusChem* **2022**, *15*, 202200348.
[9] X. Liu, J. Yi, K. Wu, Y. Jiang, Y. Liu, B. Zhao, W. Li, J. Zhang, *Nanotechnology* **2020**, *31*, 122001.
[10] T. Xue, H. J. Fan, *J. Energy Chem.* **2021**, *54*, 194.
[11] Fortune Business Insights, Alkaline Battery Market Size, Share, and Industry Analysis, By Product (Primary and Secondary), By Size (AA, AAA, 9 Volt, and Others), By Application (Remote Control, Consumer Electronics, Toys & Radios, and Others), and Regional Forecast, 2024–2032, 2024, https://www.fortunebusinessinsights.com/alkaline-battery-market-103298 (accessed: November 2024).
[12] M. B. Lim, T. N. Lambert, B. R. Chalamala, *Mater. Sci. Eng. R Rep.* **2021**, *143*, 100593.

[13] P. Ruan, S. Liang, B. Lu, H. J. Fan, J. Zhou, *Angew. Chem., Int. Ed.* **2022**, *61*, 202200598.
[14] G. Lai, P. Ruan, X. Hu, B. Lu, S. Liang, Y. Tang, J. Zhou, *J. Mater. Chem. A* **2023**, *11*, 15211.
[15] X. Cai, Y. Liu, J. Zha, F. Tan, B. Zhang, W. Yan, J. Zhao, B. Lu, J. Zhou, C. Tan, *Adv. Funct. Mater.* **2023**, *33*, 2303009.
[16] A. Guha, M. Sahoo, K. Alam, D. K. Rao, P. Sen, T. N. Narayanan, *iScience* **2022**, *25*, 104835.
[17] I. Vasiliev, B. A. Magar, J. Duay, T. N. Lambert, B. Chalamala, *J. Electrochem. Soc.* **2018**, *165*, A3517.
[18] S. W. Donne, G. A. Lawrance, D. A. Swinkels, *J. Electrochem. Soc.* **1997**, *144*, 2594,.
[19] J. W. Gallaway, B. J. Hertzberg, Z. Zhong, M. Croft, D. E. Turney, G. G. Yadav, D. A. Steingart, C. K. Erdonmez, S. Banerjee, *J. Power Sources* **2016**, *321*, 135.
[20] J. W. Gallaway, M. Menard, B. Hertzberg, Z. Zhong, M. Croft, L. A. Sviridov, D. E. Turney, S. Banerjee, D. A. Steingart, C. K. Erdonmez, *J. Electrochem. Soc.* **2015**, *162*, A162.
[21] E. Faegh, T. Omasta, M. Hull, S. Ferrin, S. Shrestha, J. Lechman, D. Bolintineanu, M. Zuraw, W. E. Mustain, *J. Electrochem. Soc.* **2018**, *165*, A2528.
[22] C. W. Lee, K. Sathiyanarayanan, S. W. Eom, H. S. Kim, M. S. Yun, *J. Power Sources* **2006**, *159*, 1474.
[23] A. Poosapati, R. B. Ambade, D. Madan, *Small* **2022**, *18*, 2103495.
[24] M.-H. Lin, C.-J. Huang, P.-H. Cheng, J.-H. Cheng, C.-C. Wang, *J. Mater. Chem. A* **2020**, *8*, 20637.
[25] K. Leng, G. Li, J. Guo, X. Zhang, A. Wang, X. Liu, J. Luo, *Adv. Funct. Mater.* **2020**, *30*, 2001317.
[26] M. Chen, J. Chen, W. Zhou, X. Han, Y. Yao, C.-P. Wong, *Adv. Mater.* *33*, 2007559.
[27] S. Chen, P. Sun, J. Humphreys, P. Zou, M. Zhang, G. Jeerh, S. Tao, *Energy Storage Mater.* **2021**, *42*, 240.
[28] Q. Li, X. Cui, Q. Pan, *ACS Appl. Mater. Interfaces* **2019**, *11*, 38762.
[29] T. Tran, H. Chung, D. Ivey, *Electrochim. Acta* **2019**, *327*, 135021.
[30] H. Miao, B. Chen, S. Li, X. Wu, Q. Wang, C. Zhang, Z. Sun, H. Li, *J. Power Sources* **2020**, *450*, 227653.
[31] Z. Pei, Z. Yuan, C. Wang, S. Zhao, J. Fei, L. Wei, J. Chen, C. Wang, R. Qi, Z. Liu, Y. Chen, *Angew. Chem., Int. Ed.* **2020**, *132*, 4823.
[32] K. Wu, J. Huang, J. Yi, X. Liu, Y. Liu, Y. Wang, J. Zhang, Y. Xia, *Adv. Energy Mater.* **2020**, *10*, 1903977.
[33] B. A. Magar, N. Paudel, T. N. Lambert, I. Vasiliev, *J. Electrochem. Soc.* **2020**, *167*, 020557.
[34] G. G. Yadav, J. W. Gallaway, D. E. Turney, M. Nyce, J. Huang, X. Wei, S. Banerjee, *Nat. Commun.* **2017**, *8*, 14424.
[35] R. Bakar, S. Darvishi, T. Li, M. Han, U. Aydemir, S. Nizamoglu, K. Hong, E. Senses, *ACS Appl. Polym. Mater.* **2022**, *4*, 179.
[36] F. Mallamace, C. Branca, M. Broccio, C. Corsaro, C.-Y. Mou, S.-H. Chen, *Proc. Natl. Acad. Sci. USA* **2007**, *104*, 18387.
[37] W. Sun, F. Wang, S. Hou, C. Yang, X. Fan, Z. Ma, T. Gao, F. Han, R. Hu, M. Zhu, C. Wang, *J. Am. Chem. Soc.* **2017**, *139*, 9775.
[38] Z. Shen, Z. Tang, C. Li, L. Luo, J. Pu, Z. Wen, Y. Liu, Y. Ji, J. Xie, L. Wang, Y. Yao, G. Hong, *Adv. Energy Mater.* **2021**, *11*, 2102055.
[39] F. Gao, B. Mei, X. Xu, J. Ren, D. Zhao, Z. Zhang, Z. Wang, Y. Wu, X. Liu, Y. Zhang, *Chem. Eng. J.* **2022**, *448*, 137742.
[40] M. Laurenti, N. Garino, S. Porro, M. Fontana, C. Gerbaldi, *J. Alloys Compd.* **2015**, *640*, 321.
[41] Y. Zhang, Y. Yan, X. Wang, G. Li, D. Deng, L. Jiang, C. Shu, C. Wang, *Chemistry* **2014**, *20*, 6126.
[42] J. Gao, M. A. Lowe, H. D. Abruna, *Chem. Mater.* **2011**, *23*, 3223.
[43] E. S. Ilton, J. E. Post, P. J. Heaney, F. T. Ling, S. N. Kerisit, *Appl. Surf. Sci.* **2016**, *366*, 475.
[44] D. Cabrera-German, G. Molar-Velázquez, G. Gómez-Sosa, W. de la Cruz, A. Herrera-Gomez, *Surf. Interface Anal.* **2017**, *49*, 1078.
[45] J. K. Seo, J. Shin, H. Chung, P. Y. Meng, X. Wang, Y. S. Meng, *J. Phys. Chem. C* **2018**, *122*, 11177.